Atmos. Chem. Phys. Discuss., 10, 21475–21519, 2010
www.atmos-chem-phys-discuss.net/10/21475/2010/
doi:10.5194/acpd-10-21475-2010
© Author(s) 2010. CC Attribution 3.0 License.

Atmospheric Chemistry and Physics Discussions

This discussion paper is/has been under review for the journal Atmospheric Chemistry and Physics (ACP). Please refer to the corresponding final paper in ACP if available.

First global distributions of methanol and formic acid retrieved from the IASI/MetOp thermal infrared sounder

A. Razavi[1], **F. Karagulian**[1,*], **L. Clarisse**[1,**], **D. Hurtmans**[1], **P. F. Coheur**[1,**], **C. Clerbaux**[2,1], **J. F. Müller**[3], **and T. Stavrakou**[3]

[1]Service de Chimie Quantique et Photophysique, Université Libre de Bruxelles (U.L.B.), Brussels, Belgium
[2]UPMC Univ. Paris 06; Université Versailles St-Quentin; CNRS/INSU, LATMOS-IPSL, Paris, France
[3]Belgian Institute for Space Aeronomy (BIRA-IASB), Brussels, Belgium
[*]now at: European Commission, Joint Research Centre(JRC), 21027 Ispra, Italy
[**]L. Clarisse and P. F. Coheur are respectively Postdoctoral Researcher and Research Associate with FRS-FNRS, Belgium

Received: 15 July 2010 – Accepted: 29 August 2010 – Published: 8 September 2010

Correspondence to: A. Razavi (arazavi@ulb.ac.be)

Published by Copernicus Publications on behalf of the European Geosciences Union.

Abstract

Methanol (CH_3OH) and formic acid (HCOOH) are among the most abundant volatile organic compounds present in the atmosphere. Their role in tropospheric chemistry stems from their influence on the oxidizing capacity of the atmosphere and, in the case of HCOOH, from its influence on the acidity of clouds and precipitation. In this work, we derive the first global distributions of these two organic species using the Infrared Atmospheric Sounding Interferometer (IASI) launched onboard the MetOp-A satellite in 2006. This paper describes the method used and provides a first critical analysis of the retrieved products. The retrieval process follows a two-step approach in which global distributions are first obtained on the basis of a simple radiance indexing (transformed into brightness temperatures), and then mapped onto column abundances using suitable conversion factors. For methanol, the factors were calculated using a complete retrieval approach in selected regions. In the case of formic acid, a different approach, which uses a set of forward simulations for representative atmospheres, has been used. In both cases, the main error sources are carefully determined: the average relative error on the column for both species is estimated to be about 50%, increasing to about 100% for the least favorable conditions. The distributions for the year 2009 are discussed in terms of seasonality and source identification. Global correlations between methanol and formic acid as well as correlations between these two species and carbon monoxide are also presented and discussed.

1 Introduction

Volatile Organic Compounds (VOCs) includes thousands of different carbon-containing gases present in our atmosphere at concentrations ranging from less than a pptv to more than a ppmv. Emitted from a large variety of processes (biogenic or anthropogenic) at the Earth's surface, they have an important influence on the atmospheric composition and climate. VOCs are precursors to tropospheric ozone (Houweling et al.,

ACPD
10, 21475–21519, 2010

1998), they play an important role on the oxidizing capacity of the troposphere (Atkinson and Arey, 2003; Monks, 2005), they lead to the formation of secondary organic aerosols (Tsigaridis and Kanakidou, 2007; Heald et al., 2008) and they impact on climate change in different indirect ways (Meinshausen et al., 2006; Feingold et al., 2003; Charlson et al., 1987). In order to better understand and quantify their emissions and the role they play in the Earth's system, it is important to assess their atmospheric distribution at the global scale.

1.1 Observation of VOCs from space

The first steps in measuring volatile organic compounds by infrared satellite sounders were made during the last years, mostly using high-sensitive limb-viewing instruments. A series of compounds, among which methanol and formic acid, have been observed in young or aged biomass burning plumes with the ACE-FTS instrument (Rinsland et al., 2004; Dufour et al., 2006; Coheur et al., 2007; Rinsland et al., 2007; Herbin et al., 2009). Large datasets of that sounder, covering several years, have been gathered to provide quasi-global distributions of these two species and to study their seasonal variability (Rinsland et al., 2006; Dufour et al., 2007; Abad et al., 2009). Similarly the observations of the MIPAS limb emission sounder have enabled mapping upper tropospheric distributions of several organic species such as PAN, HCN and C_2H_6 (Glatthor et al., 2007, 2009); very recently global distributions of formic acid have also been gathered and analyzed (Grutter et al., 2010). The possibility of probing these VOCs lower in the atmosphere using nadir infrared sounders was suggested based on local observations, both by TES (Beer et al., 2008) and IASI (Coheur et al., 2009), in the latter case in large biomass burning plumes.

Other VOCs observations from space have been performed using ultraviolet (UV) sounders. The GOME and OMI instruments provide measurements of formaldehyde (Chance et al., 2000; Millet et al., 2008b), providing constrains on the emissions of isoprene (Shim et al., 2005; Palmer et al., 2006) and other non-methane volatile organic compounds (NMVOCs) (Fu et al., 2007; Stavrakou et al., 2009). With the comple-

ACPD
10, 21475–21519, 2010

mentary use of SCIAMACHY (De Smedt et al., 2008) and with the GOME follow-on instrument onboard MetOp-A (GOME-2), a long-term dataset (14 years) of formaldehyde observations is now available. In addition, measurements of glyoxal have also been made from the SCIAMACHY instrument (Wittrock et al., 2006; Vrekoussis et al., 2009).

This study provides the first global distributions of methanol and formic acid observed by the IASI (Infrared Atmospheric Sounding Interferometer) instrument (Phulpin et al., 2007), briefly described in Sect. 2.1. This infrared nadir-looking sounder has already demonstrated its potential for the monitoring of different trace gases such as CO (George et al., 2009; Turquety et al., 2009), O_3 (Boynard et al., 2009), CH_4 (Razavi et al., 2009) and HNO_3 (Wespes et al., 2009). IASI has also demonstrated its high sensitivity to weak absorbers such as NH_3, for which global and local distributions have been obtained (Clarisse et al., 2009, 2010). The same method as the one used for retrieving global NH_3, and which relies on a simple difference of brightness temperatures, has been adapted to retrieve methanol and formic acid total columns. The method is described in Sect. 2.2 and a critical analysis of the resulting methanol field is provided in Sect. 3. The latter includes a first interpretation of the global distributions and seasonality of methanol as well as an error analysis. Section 4 provides similar analysis for formic acid. In addition, correlations between the two species and between them and CO are presented in Sect. 5.
Prior to this, a review of sources, sinks and previous measurements of methanol and formic acid is provided.

1.2 Methanol

Methanol (CH_3OH) is the most abundant organic species in the Earth's atmosphere after methane and is also the main non-methane organic volatile compound in the mid to upper troposphere (Heikes et al., 2002). Because its main removal process is oxidation by OH (Atkinson, 1986), CH_3OH has a significant impact on the oxidizing capacity of the troposphere and on the global budget of tropospheric ozone (Tie et al., 2003).

ACPD
10, 21475–21519, 2010

Additional sinks include removal by dry and wet deposition and uptake by the ocean (Jacob et al., 2005; Millet et al., 2008a). Its mean lifetime is evaluated to be about 10 days in the free troposphere. The main emission sources of methanol are biogenic processes, involving plant growth (MacDonald and Fall, 1993; Nemecek-Marshall et al., 1995; Harley et al., 2007; Galbally and Kirstine, 2002) and plant decay to a lesser extent (Warneke et al., 1999). Other sources include biomass burning (Holzinger et al., 2005), oxidation of methane and other VOCs, as well as anthropogenic emissions from vehicles and industrial activities (Singh et al., 2000). There still exists large uncertainties in the relative source strengths, the atmospheric distribution and budget of CH_3OH (Singh et al., 2000; Tie et al., 2003; Jacob et al., 2005).

During the past few years, coordinated measurements campaigns have been conducted which provide, among other trace species, in situ and aircraft determination of methanol abundances, and from there information about its different emission sources. The diurnal and seasonal cycle of CH_3OH has been studied from in situ measurement in different types of environments such as forest (Karl et al., 2003, 2005), rural (Schade and Goldstein, 2006; Brunner et al., 2007; Jordan et al., 2009) or urban areas (Filella and Peñuelas, 2006; Nguyen et al., 2001) with a variety of techniques. The concentrations usually increase during daytime and exhibit also another strong increase just after sunset because of the boundary layer squeeze. Moreover, CH_3OH abundances are found to be higher during spring because of high plant growth emissions during that season. Methanol concentrations of about 4 ppbv have been reported in the amazonian region (Karl et al., 2007; Eerdekens et al., 2009). Aircraft measurements were also carried out over oceans (Singh et al., 2000, 2004) where background concentrations of a few hundreds of pptv were found. Airborne observations led also to the study of CH_3OH in several biomass burning plumes (Yokelson et al., 1999; Fischer et al., 2003; Yokelson et al., 2003; Holzinger et al., 2005) where volume mixing ratios (vmr) of up to several tens of ppbv were found. Observations of CH_3OH with ground-based infrared spectrometers were also recently conducted in Australia (Paton-Walsh et al., 2008) and in Arizona (Rinsland et al., 2009). The latter study provides an unprecedented 22 years

ACPD
10, 21475–21519, 2010

time series of free tropospheric CH_3OH; it does not report any significant trend over the years but shows a clear seasonality with a maximum in early July and a minimum during January.

The quasi-global distributions obtained from ACE-FTS (Dufour et al., 2007) have further revealed that the surface sources of methanol have a significant impact on its upper tropospheric concentrations, which are mostly driven by biogenic and biomass burning emissions in the Northern and Southern Hemisphere, respectively.

1.3 Formic acid

Formic acid (HCOOH) is one of the most abundant organic acid and has a strong influence on pH-dependent chemical reactions in clouds (Keene and Galloway, 1988). It has also been identified as a major sink for OH reactions in cloud water (Jacob, 1986). Although its sources and sinks are still poorly quantified, HCOOH is known to be emitted by various processes: biomass burning (Goode et al., 2000; Worden et al., 1997; Yokelson et al., 1997), biogenic emissions from vegetation (Keene and Galloway, 1984, 1988), emissions from soil (Sanhueza and Andreae, 1991), from ants (Graedel and Eisner, 1988), as a secondary product from organic precursors (Rasmussen and Khalil, 1988; Arlander et al., 1990) and also from motor vehicles (Kawamura et al., 1985; Grosjean, 1989). Formic acid can be also produced from the aqueous oxidation of formaldehyde in cloud and rain water (Chameides and Davis, 1983) as well as from the oxidation of formaldehyde by HO_2 radicals in the cold tropopause region (Hermans et al., 2005). It is mainly removed from the troposphere through wet and dry deposition but also through oxidation by the OH radical to a lesser extent. The resulting lifetime of HCOOH is estimated to be a few days in the boundary layer depending highly on precipitations (Sanhueza et al., 1996). The lifetime increases in the free troposphere, due to the very low OH-oxidation rate constant. HCOOH has been found to be a product of the isoprene oxidation by ozone (Jacob and Wofsy, 1988; Martin et al., 1991) and by OH radicals, in particular through the OH-oxidation of glycolaldehyde (Butkovskaya et al., 2006a) and hydroxyacetone (Butkovskaya et al., 2006b), which

ACPD
10, 21475–21519, 2010

are two important isoprene oxidation products, but also through the OH-oxidation of isoprene nitrates (Paulot et al., 2009).

In situ measurements of formic acid in the boundary layer have been carried out using different techniques in various parts of the world, from rural sites (Talbot et al., 1988; Puxbaum et al., 1988; Talbot et al., 1990; Hartmann et al., 1991; Helas et al., 1992) to urban areas (Grosjean, 1989; Khwaja, 1995; Granby et al., 1997; Souza et al., 1999). The observed HCOOH volume mixing ratio in the boundary layer ranges from 0.01 to 10 ppbv. Its diurnal cycle shows larger concentrations in the mid- to late afternoon (Martin et al., 1991; Hartmann et al., 1991) indicating larger sources during daytime (biogenic emission, photochemical reactions) and dry deposition at nighttime.

HCOOH measurements in the upper troposphere, performed during several aircraft campaigns (Reiner et al., 1999; Jaeglé et al., 2000; Singh et al., 2000), have reported mixing ratios from about 30 to 215 pptv. HCOOH has also been probed in different biomass burning plumes (Yokelson et al., 1999; Goode et al., 2000; Herndon et al., 2007) with concentrations of around ten ppbv; Worden et al. (1997) reported HCOOH total columns of 8.6 and 11.2×10^{16} molec/cm^2 above two fire events in the USA using optical measurements in the infrared. Similar spectral measurements, which used the HCOOH ν_6 absorption band in the IR, were performed from a balloon (Goldman et al., 1984; Remedios et al., 2007), with mixing ratios up to 600 pptv at about 7 km height, or from the ground (Rinsland et al., 2004). The latter study gives insight on the seasonal variation of HCOOH, with a mean mixing ratio in the free troposphere from about 300 pptv in October–December to about 800 pptv in July–September, likely resulting from higher biogenic emissions during the growing season. Other ground-based measurements above Jungfraujoch were very recently analyzed over a 22 years period and show a similar seasonal cycle with a maximum occurring during summer as well as significant diurnal and day-to-day variability (Zander et al., 2010).

The first satellite observations in the upper troposphere were reported from the ACE-FTS instrument (Rinsland et al., 2006, 2007; Coheur et al., 2007) and were correlated to biomass burning events. Recent work performed with ACE-FTS on quasi-global ob-

ACPD
10, 21475–21519, 2010

servations of HCOOH reported an average mixing ratio of about 0.3 ppbv in the free troposphere with hot spots of up to 0.59 ppbv in tropical regions (Abad et al., 2009). Very recent global distributions were also assessed by the MIPAS sounder (Grutter et al., 2010) over a 6 years period. They report seasonal variations that may be associated to biogenic emissions with higher mixing ratios at 8 km during summer (about 100 pptv) than in winter (about 45 pptv). High concentrations were also observed in biomass burning plumes in the Southern Hemisphere. The nadir-viewing IASI sounder has also recently demonstrated the possibility to observe the HCOOH spectral signature in fire plumes (Coheur et al., 2009). In this study, we provide the first distributions of formic acid total columns above land, differentiated into four seasons for the year 2009. The retrieval method is slightly different from the one used for methanol because the conversion factor between brightness temperature differences and total columns is derived from a set of forward simulation. Details and error estimation are provided in Sect. 4.1.

It is important to note that a new set of HCOOH spectroscopic line parameters has been recently generated by Vander Auwera et al. (2007) and implemented in the latest versions of HITRAN and GEISA databases. The updated data set reports HCOOH line intensities larger by about a factor 2 compared to previous studies (Perrin and Vander Auwera, 2007). This implies that concentrations obtained from previous infrared retrievals were likely too high by the same factor.

2 Instrument and method

2.1 Description of IASI

The IASI instrument, launched onboard the MetOp-A platform in October 2006 on a polar sun-synchronous orbit, is a nadir-looking Fourier transform spectrometer that records the Earth's outgoing radiation from 645 to 2760 cm^{-1} without gaps at an apodized resolution of 0.5 cm^{-1}. Its field of view is a 2×2 matrix of circular pixels which

ACPD
10, 21475–21519, 2010

have a 12 km footprint diameter at nadir. IASI provides two global Earth coverages per day (about 1 280 000 spectra) thanks to the wide scans across its track (2200 km swaths). It offers also a very good signal-to-noise ratio, with a Noise Equivalent Delta Temperature (NEDT) at 280 K of about 0.2 K in the spectral region of interest (which extends from 975 to 1150 cm^{-1}). Moreover, with the successive launch of two other identical instruments, the IASI mission will provide consistent measurements over a 15 years period. A technical description of IASI and examples of applications for chemistry can be found in the review of Clerbaux et al. (2009). The IASI calibrated radiance spectra are disseminated in near-real time by the EumetCast system along with temperature, humidity profiles and cloud information (coverage, temperature and altitude). Only cloud free observations (when the cloud coverage for the pixel is below 2%) are taken into account for this study.

The measurement of methanol and formic acid concentrations from IASI is quite challenging due to their weak absorption and the interference of other molecules in the same spectral range (see Fig. 1). CH_3OH is observable using its C–O stretching absorption band located around 1033 cm^{-1}. The spectral range also covers the ν_6 absorption band of HCOOH located near 1105 cm^{-1} and the ν_3 band of trans–HCOOH at 1777 cm^{-1} (Perrin et al., 2009), which can't be detected in the IASI spectra because of strong water vapor interferences.

2.2 Retrieval approach

In order to take advantage of the very good spatial coverage of IASI we have chosen a simple, fast and robust approach based on brightness temperature differences (ΔT_b), similar to the method already used for the retrieval of sulfur dioxide (Clarisse et al., 2008) and ammonia (Clarisse et al., 2009). It consists in two steps: (i) the determination of ΔT_b globally and (ii) the conversion of ΔT_b to total column amounts using one (global) or two (continental and oceanic) conversion factors.

ACPD
10, 21475–21519, 2010

The ΔT_b corresponds to the difference between the brightness temperatures measured in one or several channels selected in the absorption signature of the target molecule ($T_{b,\text{target}}$) and the brightness temperature of nearby channels selected in a spectral region where the least absorptions are found ($T_{b,0}$). This is expressed in the following equation as

$$\Delta T_b = \langle T_{b,0} \rangle - \langle T_{b,\text{target}} \rangle \quad (1)$$

This quantity gives a handy estimate for the strength of absorption and hence of the concentration. However, the physics of the radiative transfer is not accounted for and the conversion of ΔT_b to total columns requires a full radiative transfer treatment. For this purpose, we have retrieved CH_3OH total columns at various locations of the world with an inversion model based on the Optimal Estimation Method (OEM) (Rodgers, 2000) that includes a line-by-line radiative transfer model. This is implemented in the *Atmosphit* software developed at the Université Libre de Bruxelles (for more information see Clarisse et al. (2008) and Coheur et al. (2005)). The method is only applied in selected regions due to computational limitations. The conversion factor derived by matching the retrieved columns on the corresponding ΔT_b is applied globally to derive the total column distributions.

For HCOOH, we used an alternative conversion method only based on forward simulations (see Sect. 4.1).

In the next two sections we describe the different retrieval parameters (the chosen channels, spectral intervals and a priori information) and present the resulting global distributions for CH_3OH and HCOOH, respectively.

ACPD
10, 21475–21519, 2010

3 Methanol retrieval and distributions

3.1 Retrieval settings

Methanol a priori profiles and covariance matrices were derived from distributions calculated by the IMAGESv2 global chemistry-transport model (Stavrakou et al., 2009). Two different vertical profiles were selected: an average continental and an average oceanic profile. This choice is justified by the existence of strong emission over continents resulting in enhanced concentrations in the boundary layer. These two profiles are illustrated on Fig. 2 together with their associated covariance matrix. The continental a priori profile has a surface mixing ratio of about 2.5 ppbv, about four times larger than in the oceanic profile. Above 4 km, the two profiles are similar with only slightly higher concentrations for the continental profile. The covariance matrices both show higher variabilities in the lower (0 to 2 km) and upper (14 to 18 km) troposphere. Over continental surfaces, the variabilities are larger by about 25%. In both cases, the correlation length is large.

As can be seen from Fig. 1, the methanol spectral signature is fully overlapped by the much stronger ozone band at 10 µm. A large spectral range is therefore needed in order to properly account for this strong interference in the retrieval process. The spectral range extending from 981.25 to 1038 cm^{-1} was selected after several tests. CH_3OH partial columns are retrieved in 4 km thick layers from the ground to 16 km. Partial columns of O_3 in 6 layers up to 42 km and the total columns of H_2O and NH_3 are simultaneously adjusted. The regions selected for the retrievals are located above Congo (0–35° S, 10–50° E), Chad (0–25° N, 0–30° E), Brazil (0–20° S, 35–60° W), India (5–40° S, 70–90° E) and the Atlantic ocean (30° S–25° N, 10–40° W). These regions were selected because of their high ΔT_b values. An example of inversion is presented on Fig. 4 (top panel) for a case where the CH_3OH signature is unambiguous. The RMS of the residue when CH_3OH is not included in the retrieval is significantly higher (3.1×10^{-6} W/m^2srm^{-1}) than when it is taken into account (2.5×10^{-6} W/m^2srm^{-1},

ACPD
10, 21475–21519, 2010

this value being very close to the theoretical noise). This specific retrieval leads to a methanol total column of 5.57×10^{16} molec/cm^2. On the bottom panel of Fig. 4, representative total column averaging kernel differentiated for continental and oceanic retrievals are illustrated. They correspond to the mean averaging kernel for all retrievals performed in the selected regions. In both cases, the sensitivity is maximum in the mid to upper troposphere from about 5 to 11 km, but retrievals over land show much higher sensitivity near the ground, largely due to the higher thermal contrast (Clerbaux et al., 2009).

For the global ΔT_b calculation, the three target channels, all chosen in the Q branch of CH_3OH (at 1033.25, 1033.5 and 1033.75 cm^{-1}, see Fig. 1), are also contaminated by O_3. Therefore, the baseline channels were also chosen inside the O_3 absorption band (at 1019, 1019.5, 1036.25, 1038, 1047 and 1048.5 cm^{-1}, see Fig. 1) in a way that maximizes the sensitivity of ΔT_b to the CH_3OH amount. To deal with the remaining contribution of O_3, the relationship between ΔT_b and O_3 concentrations has been derived using a set of forward simulations. For different columns of O_3 (ranging from 185 to 407 DU), the spectrum and ΔT_b were calculated with a fixed amount of CH_3OH (4×10^{16} molec/cm^2). The results, presented on Fig. 4 assuming a typical midlatitude summer atmosphere (1976 US standard model), show a a very well defined linear correlation between the total column of ozone and the calculated ΔT_b. Similar results were obtained for other typical atmospheres and an average linear dependence was computed (with a slope of 9.02×10^{-4}K/DU). The same type of simulations were performed to derive the influence of water vapor on the CH_3OH ΔT_b (gray curve in Fig. 4). From these relationships a corrected ΔT_b for methanol which minimizes the dependence on O_3 and H_2O is calculated as follows

$$\Delta T_b' = \Delta T_b + 9.02\times10^{-4}\, C_{O_3} + 8.13\times10^{-25}\, C_{H_2O} \quad (2)$$

where C_{O_3} and C_{H_2O} are the total columns of O_3 in Dobson unit and of H_2O expressed in molec/cm^2, respectively. This correction is applied to all observations using the total columns of O_3 and H_2O retrieved from IASI with a near-real time algorithm based on

ACPD
10, 21475–21519, 2010

the OEM.

The next step of the method, i.e. the determination of a suitable conversion factor between $\Delta T'_b$ and CH_3OH total columns, is performed based on the retrievals in selected regions of the world. Only retrievals results with a DOFS (Degrees Of Freedom for Signal, given by the trace of the averaging kernel matrix) higher than 0.75 and a RMS of the residual lower than 4×10^{-6}W/(m^{2}srm^{-1}) are taken into account. This translates to a total of 5147 and 2849 observations above land and oceans, respectively. The corresponding scatter plots are shown in Fig. 5. In both cases, a linear fit shows good correlation coefficient (about 0.75). The slope for the retrievals over land is found to be much larger than over oceans. Two different conversion factors are therefore used and applied to the $\Delta T'_b$ calculated globally:

$$C^{\text{land}}_{CH_3OH} = 4.482\times\Delta T'_b \quad (3)$$

$$C^{\text{ocean}}_{CH_3OH} = 2.987\times\Delta T'_b \quad (4)$$

where the CH_3OH total columns (C_{CH_3OH}) are expressed in 10^{16}molec/cm^2. It is important to note that for the derivation of the global distributions, only cloud free measurements recorded during daytime were taken into account. This is justified because daytime measurements are generally characterized by a positive thermal contrast and are therefore more sensitive to the lower troposphere.

3.2 Global distributions

The method proposed above allows to derive the first global distributions of methanol. In order to shed light onto seasonal variations, the four seasons have been differentiated as follows: DJF (December 2008, January 2009 and February 2009), MAM (March, April and May), JJA (June, July and August) and SON (September, October and November). The resulting distributions averaged on a $0.5^\circ\times0.5^\circ$ grid are shown in Fig. 6. Note that measurements above sand surfaces, which causes erroneous

ACPD
10, 21475–21519, 2010

high CH_3OH concentrations due to spectrally resolved surface emissivity (Wilber et al., 1999) have also been discarded.

Figure 6 shows large seasonal variations in the methanol columns. Higher concentrations are found in the northern hemisphere during spring and summer (up to 4×10^{16} molec/cm^2 in Central and Northern Asia) when vegetation is growing. In the Southern hemisphere, the highest concentrations are found during the dry season (SON) and may be related to biomass burning. CH_3OH is also observed over oceans (with values around 2×10^{16} molec/cm^2) mostly between Africa and South America but also in the whole Northern hemisphere in spring and summertime. The presence of CH_3OH in remote oceanic regions is probably largely due to transport of continental emissions although oceanic emissions (Millet et al., 2008a) and the ubiquitous methane oxidation might also contribute. Methanol total columns range from about 0.01×10^{16} molec/cm^2 above sea surfaces to 5.40×10^{16} molec/cm^2 over large emission regions.

During the Northern Hemispheric winter (DJF), methanol hot spots of low intensity are found in the Southern Hemisphere (South America, South Africa and Western Australia) above vegetated areas where CH_3OH emissions may be related to plant growth. When comparing the distribution with AATSR (Arino et al., 2005) fire count maps, we find a high degree of coincidence in Africa between 5 and 15° N, suggesting a possible biomass burning contribution. During springtime (MAM), this specific region is subject to enhanced CH_3OH columns which is possibly due to an increase in the fire numbers and intensities. Strong enhancements are also observed over India and to a lesser extent over Burma, Manchuria and Mexico, which can be at least partly related to biomass burning. In contrast, biomass burning is unlikely to be a dominant source in the Northern Hemisphere except in some regions (Kazakhstan, East Russia, Alaska) during JJA. It can be seen that CH_3OH concentrations are progressively increasing from winter (DJF) to summertime (JJA). This can be explained by the seasonal cycle of the vegetation source which presents a maximum in late spring (Schade and Goldstein, 2006; Rinsland et al., 2009). During fall (SON), CH_3OH concentrations decrease again

ACPD
10, 21475–21519, 2010

in the Northern Hemisphere and increase in the Southern Hemisphere. Again, biomass burning is likely responsible for the strong enhancements in South America, Congo and Northern Australia.

Although biomass burning is assumed to be a weak emission source of methanol (accounting for about 5% of total emissions according to current inventories), the main hot spots in the global distributions appear to be possibly related to fires, indicating a possible underestimation of the biomass burning source in models. Caution is required, however, because pyrogenic methanol is usually transported higher in the troposphere where the IASI sensitivity is larger. This is consistent with the fact that biomass burning has been found to be a significant source of methanol in the upper troposphere (Dufour et al., 2007). The assimilation of IASI data into models should help determining the respective contributions of biogenic and fire emissions to the global methanol budget.

3.3 Error assessment

One of the disadvantages of the method described above is that it does not provide an estimation of the systematic errors associated with the retrieved total columns. Because we are deriving the CH_3OH columns from a weak signal, the associated error is expected to be quite large. An estimation of the error on the CH_3OH columns derived from IASI can be based on forward simulations. For this purpose, we used a large set of different atmospheres compiled in an ECMWF database (Chevallier, 2001). Different input profiles are used for CH_3OH, corresponding to the different continental profiles taken from the IMAGESv2 model. The total columns used as input for the simulations are then compared to those retrieved from the simulated spectra using the same method as described above. The difference between the two columns gives a fair estimate of the absolute column errors.

It turns out that this absolute difference increases when the amount of CH_3OH in the boundary layer (between the surface and 3 km height) increases. It follows that the high concentrations of methanol in the boundary layer (close to the emission sources) will not be well reproduced by the ΔT_b method. This is consistent with the averaging ker-

ACPD
10, 21475–21519, 2010

nel shape and the well known limited sensitivity of the infrared measurements toward low altitudes. Figure 7 shows the histogram of the relative difference between the total columns used as input in the forward simulations and the calculated ones. The distribution is similar to a normal distribution with a mean very close to zero (0.6%). The standard deviation (48.9%) provides our best estimate of the relative error on the retrieved methanol total column. This value is, however, clearly a lower bound for regions located close to emission sources and with low thermal contrast. In these regions, based on our analysis, errors as high as 100% are likely.

4 Formic acid retrieval and distributions

4.1 Retrieval settings and errors

In the case of formic acid, the target channel for brightness temperature has been chosen in the Q-branch at 1105.0 cm^{-1} which is the strongest absorption feature detectable in the IASI spectrum. The reference channels were chosen on both sides at 1103.0 and 1109.0 cm^{-1}. The ΔT_b values computed globally over one year range from about 0 to 5 K. As there exist large uncertainties on the vertical profile of formic acid, we have chosen here to rely on a composite vertical profile for the a priori. It was built from aircraft measurements for the low and free troposphere and from ACE-FTS for the upper troposphere. Also, because the lifetime of HCOOH is short and there is no known emissions from oceans, we have chosen to limit the analysis to continental profiles. The a priori profile is an average of profiles collected over the USA (25–55° N, 230–290° E) including (i) aircraft data from the INTEX-B C-130 campaign in April and May 2006 (Kleb et al., 2010) between 0–5 km, (ii) the arithmetic mean between INTEX-B data and ACE-FTS data (Abad et al., 2009) measured from March to May for altitudes between 6 and 8 km, (iii) and an averaged ACE-FTS profile between 9 and 11 km. The resulting profile, illustrated in Fig. 8, has a surface mixing ratio of about 750 pptv, which smoothly decreases as the altitude increases, down to less than 100 pptv above 7 km. Concentration above 11 km have been linearly extrapolated up to 20 km.

ACPD
10, 21475–21519, 2010

As in the case of methanol, conversion factors between the ΔT_b and the HCOOH total columns were tentatively derived based on OEM retrievals in selected regions around the world. Because of the weak signal and the presence of water vapor interferences, the retrievals are unstable and lead to large errors. Forward simulations using the ECMWF database and varying the HCOOH concentrations (scaling of the profile) were conducted (as for CH_3OH) to compute absolute errors as the difference between the true columns (input of the forward model) and those retrieved from the ΔT_b. Figure 9 illustrates in gray the histogram of the relative errors. The mode of the errors is at about 60.0% suggesting a strong bias between the calculated and simulated total columns. Therefore, an alternative method has been used to derive the conversion factor between the ΔT_b and the total columns. Relying only on the forward calculations, it minimizes also the dependence upon the water vapor content (C_{H_2O} expressed in molec/cm^2) and accounts for the varying sensitivity of the measurement to the local thermal contrast (τ). The following equation is used

$$C_{\mathrm{HCOOH}} = \frac{\Delta T_b - b_1\tau - b_2\tau C_{\mathrm{H_2O}} - c_1 C_{\mathrm{H_2O}} - c_2}{a_1\tau + a_2\tau C_{\mathrm{H_2O}}} \quad (5)$$

with the parameters :

$a_1 = 0.024$, $a_2 = 4\times10^{-26}$,
$b_1 = 0.005$, $b_2 = 1\times10^{-26}$,
$c_1 = 0.131\times10^{-23}$, $c_2 = 0.139$,

and where HCOOH total columns (C_{HCOOH}) are expressed in 10^{16} molec/cm^2. This mapping of ΔT_b onto total columns of HCOOH provides much better results. However a significant dependency on the thermal contrast remains, with lower errors found for higher thermal contrast values. Although it may be a quite conservative criterion, we have chosen to consider only the cases for which the thermal contrast is higher than 5K. The resulting histogram of the relative errors between the simulated and calculated

ACPD
10, 21475–21519, 2010

HCOOH total columns is shown in black on Fig. 9. It is similar to a normal distribution, with its mean being equal to −0.8%. Our estimation of the error on the formic acid total column is given by the standard deviation of the errors, which is about 60%. This error is only slightly higher than the error found for the CH_3OH columns, but only applies here to favorable situations with large thermal contrast.

4.2 Global distributions

The global distributions of formic acid for the four seasons are illustrated in Fig. 10, on a 0.5°×0.5° averaged grid. Only cloud free observations recorded during daytime and with a thermal contrast higher or equal to 5K were taken into account. The latter constrain removes unfortunately many observations at high latitudes (no observations above about 45° N in winter and about 65° N during summer). Grid points which include less than ten HCOOH measurements were also filtered out. As for CH_3OH, clear seasonal variations are observed. The retrieved HCOOH total columns range from background values of less than 0.5×10^{16} molec/cm^2 above Europe and North America to 5×10^{16} molec/cm^2 above fire events, mainly during summer 2009 in Africa. These high formic acid total columns in fire plumes are in good agreement with the values reported by Coheur et al. (2009) and Worden et al. (1997) if we account for the factor 2 resulting from the use of the improved line parameters (Vander Auwera et al., 2007).

The 2009 northern hemispheric winter season (DJF) shows the lowest number of observations. During that period, enhancements of HCOOH which might be partly due to biomass burning are detected in the western-central region of Africa and to a lesser extent in South America. During spring (MAM), we observe a decrease in the HCOOH total columns above Africa and South America. High concentrations are also found in Asia (India, Burma and Manchuria) which are well correlated with CH_3OH hot spots. The peak of the biomass burning season in South America and Southern Africa happens usually around August–September whereas in Australia most of the burning occurs around October–November (Gloudemans et al., 2006). Together with the minimal washout of HCOOH occurring during the dry season, it probably largely

ACPD
10, 21475–21519, 2010

explains the high HCOOH total columns observed during JJA above Congo and Brazil as well as in Northern Australia during the SON period. Other regions of high HCOOH columns can be associated to boreal fires during the JJA period such as Eastern Russia and some regions of North America. Large HCOOH columns are also observed on the East coast of North America and in East China. They might partly be due to anthropogenic activities. Finally, the very widespread hot spots found during SON above Amazonia and Central Africa do not seem to be related to fires and very likely points to biogenic emissions of either HCOOH or HCOOH precursors. Several common patterns are found in the distributions of HCOOH and CH_3OH columns, probably due to their common emission sources (such as biomass burning and plant growth). Also note that the seasonality observed here is in good agreement with that reported from ACE-FTS (Abad et al., 2009) and from MIPAS (Grutter et al., 2010).

5 Correlations

In this section, we present a first analysis of the global correlations between methanol and formic acid as well as an example of global correlation of these two species with the IASI CO total columns (George et al., 2009) for the 2009 summer period (JJA) when biogenic emissions are largest in the Northern Hemisphere. The scatter distributions between CH_3OH and HCOOH total columns, shown in Fig. 11, are differentiated into four seasons in the same way as done before for their global distributions. For each season, methanol total columns are found to be generally higher than the formic acid columns. The DJF and SON periods show very similar linear relationships with good correlation coefficients (about 0.70), confirming the similarities between their emission sources observed in the global distributions. The correlations in spring (MAM) and summer (JJA) are slightly worse with coefficients of about 0.6 and 0.4, respectively. Their slopes are also found to be lower (about 0.4 for MAM and JJA against 0.75 for DJF and SON) indicating higher emission of CH_3OH than HCOOH from plant growth in the Northern Hemisphere. During JJA and SON, cases with relatively higher HCOOH

ACPD
10, 21475–21519, 2010

concentrations compared to CH_3OH are found, which are mostly located in the Southern Hemisphere, in regions affected by biomass burning.

Concerning the correlations with carbon monoxide, different studies have already demonstrated the relationship between VOCs and CO inside fire plumes (Yokelson et al., 1999; Goode et al., 2000; Coheur et al., 2009). Figure 12 shows the relationship of CO with CH_3OH (top panel) and HCOOH (bottom panel) for all observations above land surfaces during JJA. The colors discriminate between different latitudinal bands of 20° width. The black line represents the correlation between the two species in biomass burning plumes (inferred over selected fire regions identified with the AATSR fire data and mostly located above Africa, between 25°S and 10° N). In this way, observations influenced by biomass burning can clearly be identified on each plot and are found to be mostly located in the tropical belt. Methanol and formic acid north of 40° N (orange and red) are higher than the biomass burning line. This suggests that at these latitudes, HCOOH and CH_3OH are mostly emitted by biogenic processes. When comparing HCOOH with CO, most points located at mid northern latitude (between 20° N and 40° N, in yellow) present a much lower ratio than for biomass burning. For CH_3OH, these points are however well correlated to biomass burning. Further work is needed to assess the usefulness of the ratios between these VOCs and CO to discriminate specific emission processes.

6 Conclusions and perspectives

In this study, we have retrieved methanol and formic acid from the data provided by the IASI sounder. Using a radiance indexing method and the calculation of brightness temperature differences, first global distributions are computed. They are provided as total columns, after careful conversion of the brightness temperature differences. The conversion has been achieved based on a set of retrievals in selected regions for methanol and on forward simulations for formic acid. Taking full advantage of the IASI spatial and temporal coverage, unprecedented information on the location and origin

ACPD
10, 21475–21519, 2010

of sources have been acquired.

The simple retrieval method used here does not allow the determination of individual error for each observations. We have estimated, using a large set of representative forward calculation, global errors of about typically 50% and 60% for the methanol and formic acid total columns, respectively. Although these errors are significant, this robust method takes advantage of the very large number of IASI measurements at low computational cost. In this way, we provide global observations for these two volatile organic compounds.

The global distributions shown in this study highlight strong seasonal variations for methanol and formic acid with maximum total columns values evaluated at 5.4 and 5.0×10^{16} molec/cm^2, respectively. The strong enhancements seen in the global maps can be largely attributed to biomass burning (mostly in tropical regions). The main seasonal patterns, especially at mid-latitudes where we find higher columns in spring and summer, can be explained by variations in biogenic emissions and increased plant growth. Anthropogenic emissions could not been clearly identified in these distributions.

Methanol and formic acid were shown to be fairly well correlated, with correlation coefficient ranging from 0.4 to 0.7 depending on the season. This highlights the potential similarities between their emission sources. For summer 2009, the correlations between the two species and carbon monoxide are also presented. It suggests interestingly that the use of VOCs/CO ratios could help to differentiate the emissions of CH_3OH and HCOOH from biomass burning and biogenic sources.

It is anticipated that the assimilation of these data in a global chemistry model will help to improve the determination of the emission fluxes for these two species.

Acknowledgements. IASI has been developed and built under the responsibility of the Centre National d'Etudes Spatiales (CNES, France). It is flown onboard the MetOp satellites as part of the EUMETSAT Polar System. The IASI L1 data are received through the EUMETCast near real time data distribution service. The research in Belgium was funded by the "Communauté Française de Belgique – Actions de Recherche Concertées", the Fonds National de

ACPD

10, 21475–21519, 2010

la Recherche Scientifique (FRS-FNRS F.4511.08), the Belgian Science Policy Office and the European Space Agency (ESA-Prodex C90-327). The ACE mission is funded primarily by the Canadian Space Agency.

References

Abad, G. G., Bernath, P. F., Boone, C. D., McLeod, S. D., Manney, G. L., and Toon, G. C.: Global distribution of upper tropospheric formic acid from the ACE-FTS, Atmos. Chem. Phys., 9, 8039–8047, doi:10.5194/acp-9-8039-2009, 2009. 21477, 21482, 21490, 21493

Arino, O., Plummer, S., and Defrenne, D.: Fire disturbance: the ten years time series of the ATSR World Fire Atlas, in: ATSR Workshop, 26–30, 2005. 21488

Arlander, D., Cronn, D., Farmer, J., Menzia, F., and Westberg, H.: Gaseous oxygenated hydrocarbons in the remote marine troposphere, J. Geophys. Res., 95, 16391–16403, 1990. 21480

Atkinson, R.: Kinetics and mechanisms of the gas-phase reactions of the hydroxyl radical with organic compounds under atmospheric conditions, Chem. Rev., 86, 69–201, 1986. 21478

Atkinson, R. and Arey, J.: Atmospheric degradation of volatile organic compounds, Chem. Rev., 103, 4605–4638, 2003. 21477

Beer, R., Shephard, M., Kulawik, S., Clough, S., Eldering, A., Bowman, K., Sander, S., Fisher, B., Payne, V., Luo, M., Osterman, G., and Worden, J.: First satellite observations of lower tropospheric ammonia and methanol, Geophys. Res. Lett., 35, L09801, doi:10.1029/2008GL033642, 2008. 21477

Boynard, A., Clerbaux, C., Coheur, P.-F., Hurtmans, D., Turquety, S., George, M., Hadji-Lazaro, J., Keim, C., and Mayer-Arnek, J.: Measurements of total and tropospheric ozone from the IASI instrument: comparison with satellite and ozone sonde observations, Atmos. Chem. Phys., 9, 6255–6271, doi:10.5194/acp-9-6255-2009, 2009. 21478

Brunner, A., Ammann, C., Neftel, A., and Spirig, C.: Methanol exchange between grassland and the atmosphere, Biogeosciences, 4, 395–410, doi:10.5194/bg-4-395-2007, 2007. 21479

Butkovskaya, N., Pouvesle, N., Kukui, A., and Le Bras, G.: Mechanism of the OH-Initiated Oxidation of Glycolaldehyde over the Temperature Range 233-296 K, J. Phys. Chem. A, 110, 13492–13499, 2006a. 21480

Butkovskaya, N., Pouvesle, N., Kukui, A., Mu, Y., and Le Bras, G.: Mechanism of the OH-

ACPD

10, 21475–21519, 2010

Initiated Oxidation of Hydroxyacetone over the Temperature Range 236-298 K, J. Phys. Chem. A, 110, 6833–6843, 2006b. 21480
Chameides, W. and Davis, D.: Aqueous-phase source of formic acid in clouds., Nature, 304, 427–429, 1983. 21480
Chance, K., Palmer, P. I., Spurr, R. J., Martin, R., Kurosu, T. P., and Jacob, D. J.: Satellite observations of formaldehyde over North America from GOME, Geophys. Res. Lett., 27, 3461–3464, 2000. 21477
Charlson, R., Lovelock, J., Andreae, M., and Warren, S.: Oceanic phytoplankton, atmospheric sulphur, cloud albedo and climate, Nature, 326, 16, 1987. 21477
Chevallier, F.: Sampled databases of 60-level atmospheric profiles from the ECMWF analysis, Tech. Rep. Research Report No. 4, Eumetsat/ECMWF SAF Programme, 2001. 21489
Clarisse, L., Coheur, P.-F., Prata, A. J., Hurtmans, D., Razavi, A., Hadji-Lazaro, J., Clerbaux, C., and Phulpin, T.: Tracking and quantifying volcanic SO_2 with IASI, the September 2007 eruption at Jebel-at-Tair, Atmos. Chem. Phys., 8, 7723–7734, doi:10.5194/acp-8-7723-2008, 2008. 21483, 21484
Clarisse, L., Clerbaux, C., Dentener, F., Hurtmans, D., and Coheur, P.-F.: Global ammonia distribution derived from infrared satellite observations, Nat. Geosci., 2, 479–483, doi:doi:10.1038/ngeo551, 2009. 21478, 21483
Clarisse, L., Shephard, M., Dentener, F., Hurtmans, D., Cady-Pereira, K., Karagulian, F., Van Damme, M., Clerbaux, C., and Coheur, P.-F.: Satellite monitoring of ammonia: A case study of the San Joaquin Valley, J. Geophys. Res., in press, 2010. 21478
Clerbaux, C., Boynard, A., Clarisse, L., George, M., Hadji-Lazaro, J., Hurtmans, D., Herbin, H., Pommier, M., Razavi, A., Turquety, S., Wespes, C., and Coheur, P.-F.: Monitoring of atmospheric composition using the thermal infrared IASI/METOP sounder, Atmos. Chem. Phys., 9, 6041–6054, doi:10.5194/acp-9-6041-2009, 2009. 21483, 21486
Coheur, P., Herbin, H., Clerbaux, C., Hurtmans, D., Wespes, C., Carleer, M., Turquety, S., Rinsland, C., Remedios, J., Hauglustaine, D., Boone, C., and P.F., B.: ACE-FTS observation of a young biomass burning plume: first reported measurements of C_2H_4, C_3H_6O, H_2CO and PAN by infrared occultation from space, Atmos. Chem. Phys., 7, 5437–5446, doi:10.5194/acp-7-5437-2007, 2007. 21477, 21481
Coheur, P.-F., Barret, B., Turquety, S., Hurtmans, D., Hadji-Lazaro, J., and Clerbaux, C.: Retrieval and characterization of ozone vertical profiles from a thermal infrared nadir sounder, J. Geophys. Res., 5, 4599–4639, 2005. 21484

ACPD
10, 21475–21519, 2010

Coheur, P.-F., Clarisse, L., Turquety, S., Hurtmans, D., and Clerbaux, C.: IASI measurements of reactive trace species in biomass burning plumes, Atmos. Chem. Phys., 9, 5655–5667, doi:10.5194/acp-9-5655-2009, 2009. 21477, 21482, 21492, 21494

De Smedt, I., Müller, J., Stavrakou, T., van der A, R., Eskes, H., and Van Roozendael, M.: Twelve years of global observations of formaldehyde in the troposphere using GOME and SCIAMACHY sensors, Atmos. Chem. Phys., 8, 4947–4963, doi:10.5194/acp-8-4947-2008, 2008. 21478

Dufour, G., Boone, C. D., Rinsland, C. P., and Bernath, P. F.: First space-borne measurements of methanol inside aged southern tropical to mid-latitude biomass burning plumes using the ACE-FTS instrument, Atmos. Chem. Phys., 6, 3463–3470, doi:10.5194/acp-6-3463-2006, 2006. 21477

Dufour, G., Szopa, S., Hauglustaine, D. A., Boone, C. D., Rinsland, C. P., and Bernath, P. F.: The influence of biogenic emissions on upper-tropospheric methanol as revealed from space, Atmos. Chem. Phys., 7, 6119–6129, doi:10.5194/acp-7-6119-2007, 2007. 21477, 21480, 21489

Eerdekens, G., Ganzeveld, L., Vilà-Guerau de Arellano, J., Klüpfel, T., Sinha, V., Yassaa, N., Williams, J., Harder, H., Kubistin, D., Martinez, M., et al.: Flux estimates of isoprene, methanol and acetone from airborne PTR-MS measurements over the tropical rainforest during the GABRIEL 2005 campaign, Atmos. Chem. Phys., 9, 4207–4227, doi:10.5194/acp-9-4207-2009, 2009. 21479

Feingold, G., Eberhard, W., Veron, D., and Previdi, M.: First measurements of the Twomey indirect effect using ground-based remote sensors, Geophys. Res. Lett., 30, 1287, doi:10.1029/2002GL016633, 2003. 21477

Filella, I. and Peñuelas, J.: Daily, weekly, and seasonal time courses of VOC concentrations in a semi-urban area near Barcelona, Atmos. Environ., 40, 7752–7769, 2006. 21479

Fischer, H., de Reus, M., Traub, M., Williams, J., Lelieveld, J., de Gouw, J., Warneke, C., Schlager, H., Minikin, A., Scheele, R., and Siegmund, P.: Deep convective injection of boundary layer air into the lowermost stratosphere at midlatitudes, Atmos. Chem. Phys., 3, 739–745, doi:10.5194/acp-3-739-2003, 2003. 21479

Fu, T., Jacob, D., Palmer, P., Chance, K., Wang, Y., Barletta, B., Blake, D., Stanton, J., and Pilling, M.: Space-based formaldehyde measurements as constraints on volatile organic compound emissions in east and south Asia and implications for ozone, J. Geophys. Res., 112, D06312, doi:10.1029/2006JD007853, 2007. 21477

ACPD
10, 21475–21519, 2010

Galbally, I. and Kirstine, W.: The production of methanol by flowering plants and the global cycle of methanol, J. Atmos. Chem., 43, 195–229, 2002. 21479

George, M., Clerbaux, C., Coheur, P.-F., Hadji-Lazaro, J., Hurtmans, D., Pommier, M., Turquety, S., Edwards, D., Worden, H., Luo, M., Rinsland, C. P., and Barnet, C.: Carbon monoxide distributions from the IASI/METOP mission : evaluation with other spaceborne remote sensors, Atmos. Chem. Phys., 9, 8317–8330, doi:10.5194/acp-9-8317-2009, 2009. 21478, 21493

Glatthor, N., Von Clarmann, T., Fischer, H., Funke, B., Grabowski, U., Höpfner, M., Kellmann, S., Kiefer, M., Linden, A., Milz, M., et al.: Global peroxyacetyl nitrate(PAN) retrieval in the upper troposphere from limb emission spectra of the Michelson Interferometer for Passive Atmospheric Sounding (MIPAS), Atmos. Chem. Phys., 7, 2775–2787, doi:10.5194/acp-7-2775-2007, 2007. 21477

Glatthor, N., Von Clarmann, T., Stiller, G., Funke, B., Koukouli, M., Fischer, H., Grabowski, U., Höpfner, M., Kellmann, S., and Linden, A.: Large-scale upper tropospheric pollution observed by MIPAS HCN and C_2H_6 global distributions, Atmos. Chem. Phys., 9, 9619–9634, doi:10.5194/acp-9-9619-2009, 2009. 21477

Gloudemans, A., Krol, M., Meirink, J., De Laat, A., Van der Werf, G., Schrijver, H., Van den Broek, M., and Aben, I.: Evidence for long-range transport of carbon monoxide in the Southern Hemisphere from SCIAMACHY observations, Geophys. Res. Lett., 33, 16807, doi:10.1029/2006GL026804, 2006. 21492

Goldman, A., Murcray, F., Murcray, D., and Rinsland, C.: A search for formic acid in the upper troposphere: A tentative identification of the 1105 cm^{-1} ν_6 band Q branch in highresolution balloon-borne solar absorption spectra, Geophys. Res. Lett, 11, 307–310, 1984. 21481

Goode, J., Yokelson, R., Ward, D., Susott, R., Babbitt, R., Davies, M., and Hao, W.: Measurements of excess O_3, CO_2, CO, CH_4, C_2H_4, C_2H_2, HCN, NO, NH_3, HCOOH, CH_3COOH, HCHO, and CH_3OH in 1997 Alaskan biomass burning plumes by airborne Fourier transform infrared spectroscopy (AFTIR), J. Geophys. Res., 105, 22147, doi:10.1029/2000JD900287, 2000. 21480, 21481, 21494

Graedel, T. and Eisner, T.: Atmospheric formic acid from formicine ants: a preliminary assessment, Tellus B, 40, 335–339, 1988. 21480

Granby, K., Christensen, C., and Lohse, C.: Urban and semi-rural observations of carboxylic acids and carbonyls, Atmos. Environ., 31, 1403–1415, 1997. 21481

Grosjean, D.: Organic acids in southern California air: ambient concentrations, mobile source emissions, in situ formation and removal processes, Environ. Sci. Technol., 23, 1506–1514,

ACPD
10, 21475–21519, 2010

1989. 21480, 21481
Grosjean, D.: Formic acid and acetic acid measurements during the Southern California Air Quality Study, Atmos. Environ., 24, 2699–2702, 1990.
Grutter, M., Glatthor, N., Stiller, G., Fischer, H., Grabowski, U., Höpfner, M., Kellmann, S., Linden, A., and von Clarmann, T.: Global distribution and variability of formic acid as observed by MIPAS-ENVISAT, J. Geophys. Res., 115, D10303, doi:10.1029/2009JD012980, 2010. 21477, 21482, 21493
Harley, P., Greenberg, J., Niinemets, U., and Guenther, A.: Environmental controls over methanol emission from leaves, Biogeosciences, 4, 1083–1099, doi:10.5194/bg-4-1083-2007, 2007. 21479
Hartmann, W., Santana, M., Hermoso, M., Andreae, M., and Sanhueza, E.: Diurnal cycles of formic and acetic acids in the northern part of the Guayana shield, Venezuela, J. Atmos. Chem., 13, 63–72, 1991. 21481
Heald, C., Henze, D., Horowitz, L., Feddema, J., Lamarque, J., Guenther, A., Hess, P., Vitt, F., Seinfeld, J., Goldstein, A., and Fung, I.: Predicted change in global secondary organic aerosol concentrations in response to future climate, emissions, and land use change, J. Geophys. Res., 113, D05211, doi:10.1029/2007JD009092, 2008. 21477
Heikes, B., Chang, W., Pilson, M., Swift, E., Singh, H., Guenther, A., Jacob, D., Field, B., Fall, R., Riemer, D., et al.: Atmospheric methanol budget and ocean implication, Global Biogeochem. Cy., 16, 1133, doi:10.1029/2002GB001895, 2002. 21478
Helas, G., Bingemer, H., and Andrea, M.: Organic acids over equatorial Africa - Results from DECAFE 88, J. Geophys. Res., 97, 6187–6193, 1992. 21481
Herbin, H., Hurtmans, D., Clarisse, L., Turquety, S., Clerbaux, C., Rinsland, C., Boone, C., Bernath, P., and Coheur, P.: Distributions and seasonal variations of tropospheric ethene (C_2H_4) from Atmospheric Chemistry Experiment (ACE-FTS) solar occultation spectra, Geophys. Res. Lett., 36, L04801, doi:10.1029/2008GL036338, 2009. 21477
Hermans, I., Müller, J., Nguyen, T., Jacobs, P., and Peeters, J.: Kinetics of [alpha]-Hydroxyalkylperoxyl Radicals in Oxidation Processes. HO_2•-Initiated Oxidation of Ketones/Aldehydes near the Tropopause, J. Phys. Chem., 109, 4303–4311, 2005. 21480
Herndon, S., Zahniser, M., Nelson Jr, D., Shorter, J., McManus, J., Jiménez, R., Warneke, C., and de Gouw, J.: Airborne measurements of HCHO and HCOOH during the New England Air Quality Study 2004 using a pulsed quantum cascade laser spectrometer, J. Geophys. Res., 112, D10S03, doi:10.1029/2006JD007600, 2007. 21481

ACPD
10, 21475–21519, 2010

Holzinger, R., Williams, J., Salisbury, G., Klüpfel, T., De Reus, M., Traub, M., Crutzen, P., and Lelieveld, J.: Oxygenated compounds in aged biomass burning plumes over the Eastern Mediterranean: evidence for strong secondary production of methanol and acetone, Atmos. Chem. Phys., 4, 6321–6340, doi:10.5194/acp-4-6321-2005, 2005. 21479

Houweling, S., Dentener, F., and Lelieveld, J.: The impact of nonmethane hydrocarbon compounds on tropospheric photochemistry, J. Geophys. Res., 103, 673–10, 1998. 21476

Jacob, D.: Chemistry of OH in remote clouds and its role in the production of formic acid and peroxymonosulfate, J. Geophys. Res., 91, 9807–9826, 1986. 21480

Jacob, D. and Wofsy, S.: Photochemistry of biogenic emissions over the Amazon forest, J. Geophys. Res., 93, 1477–1486, 1988. 21480

Jacob, D., Field, B., Li, Q., Blake, D., de Gouw, J., Warneke, C., Hansel, A., Wisthaler, A., Singh, H., and Guenther, A.: Global budget of methanol: Constraints from atmospheric observations, J. Geophys. Res., 110, D08303, doi:10.1029/2004JD005172, 2005. 21479

Jaeglé, L., Jacob, D., Brune, W., Faloona, I., Tan, D., Heikes, B., Kondo, Y., Sachse, G., Anderson, B., Gregory, G., Singh, H., Pueschel, R., Ferry, G., Blake, D., and Shetter, R. E.: Photochemistry of HO_x in the upper troposphere at northern midlatitudes, Environ. Sci. Technol., 105(D3), 3877–3892, 2000. 21481

Jordan, C., Fitz, E., Hagan, T., Sive, B., Frinak, E., Haase, K., Cottrell, L., Buckley, S., and Talbot, R.: Long-term study of VOCs measured with PTR-MS at a rural site in New Hampshire with urban influences, Atmos. Chem. Phys., 9, 4677–4697, doi:10.5194/acp-9-4677-2009, 2009. 21479

Karl, T., Guenther, A., Spirig, C., Hansel, A., and Fall, R.: Seasonal variation of biogenic VOC emissions above a mixed hardwood forest in northern Michigan, Geophys. Res. Lett., 30, 2186, doi:10.1029/2003GL018432, 2003. 21479

Karl, T., Harley, P., Guenther, A., Rasmussen, R., Baker, B., Jardine, K., and Nemitz, E.: The bidirectional exchange of oxygenated VOCs between a loblolly pine (*Pinus taeda*) plantation and the atmosphere, Atmos. Chem. Phys., 5, 3015–3031, doi:10.5194/acp-5-3015-2005, 2005. 21479

Karl, T., Guenther, A., Yokelson, R., Greenberg, J., Potosnak, M., Blake, D., and Artaxo, P.: The tropical forest and fire emissions experiment: Emission, chemistry, and transport of biogenic volatile organic compounds in the lower atmosphere over Amazonia, J. Geophys. Res., 112, D18302, doi:10.1029/2007JD008539, 2007. 21479

Kawamura, K., Ng, L., and Kaplan, I.: Determination of organic acids (C_1-C_{10}) in the atmo-

ACPD
10, 21475–21519, 2010

sphere, motor exhausts, and engine oils, Environ. Sci. Technol., 19, 1082–1086, 1985. 21480
Keene, W. and Galloway, J.: Organic acidity in precipitation of North America, Atmos. Environ., 18, 2491–2497, 1984. 21480
Keene, W. and Galloway, J.: The biogeochemical cycling of formic and acetic acids through the troposphere: An overview of current understanding, Tellus B, 40, 322–334, 1988. 21480
Khwaja, H.: Atmospheric concentrations of carboxylic acids and related compounds at a semi-urban site, Atmos. Environ., 29, 127–139, 1995. 21481
Kleb, M., Chen, G., Crawford, J., Flocke, F., and Brown, C.: An overview of measurement comparisons from the INTEX-B/MILAGRO airborne field campaign, Atmos. Meas. Tech. Discuss., 3, 2275–2316, doi:10.5194/amtd-3-2275-2010, 2010. 21490
MacDonald, R. and Fall, R.: Detection of substantial emissions of methanol from plants to the atmosphere, Atmos. Environ., 27, 1709–1713, 1993. 21479
Martin, R., Westberg, H., Allwine, E., Ashman, L., Farmer, J., and Lamb, B.: Measurement of isoprene and its atmospheric oxidation products in a central Pennsylvania deciduous forest, J. Atmos. Chem., 13, 1–32, 1991. 21480, 21481
Meinshausen, M., Hare, B., Wigley, T., Van Vuuren, D., Den Elzen, M., and Swart, R.: Multi-gas emissions pathways to meet climate targets, Clim. Change, 75, 151–194, 2006. 21477
Millet, D., Jacob, D., Custer, T., de Gouw, J., Goldstein, A., Karl, T., Singh, H., Sive, B., Talbot, R., Warneke, C., and Williams, J.: New constraints on terrestrial and oceanic sources of atmospheric methanol, Atmos. Chem. Phys., 8, 6887–6905, doi:10.5194/acp-8-6887-2008, 2008a. 21479, 21488
Millet, D., Jacob, D., Folkert Boersma, K., Fu, T.-M., Kurosu, T., Chance, K., Heald, C., and Guenther, A.: Spatial distribution of isoprene emissions from North America derived from formaldehyde column measurements by the OMI satellite sensor, J. Geophys. Res., 113, D02307, doi:doi:10.1029/2007JD008950, 2008b. 21477
Monks, P.: Gas-phase radical chemistry in the troposphere, Chem. Soc. Rev., 34, 376–395, 2005. 21477
Nemecek-Marshall, M., MacDonald, R., Franzen, J., Wojciechowski, C., and Fall, R.: Methanol emission from leaves (enzymatic detection of gas-phase methanol and relation of methanol fluxes to stomatal conductance and leaf development), Plant Physiol., 108, 1359–1368, 1995. 21479
Nguyen, H., Takenaka, N., Bandow, H., Maeda, Y., de Oliva, S., Botelho, M., and Tavares, T.:

ACPD
10, 21475–21519, 2010

Atmospheric alcohols and aldehydes concentrations measured in Osaka, Japan and in Sao Paulo, Brazil, Atmos. Environ., 35, 3075–3083, 2001. 21479
Palmer, P., Abbot, D., Fu, T., Jacob, D., Chance, K., Kurosu, T., Guenther, A., Wiedinmyer, C., Stanton, J., Pilling, M., et al.: Quantifying the seasonal and interannual variability of North American isoprene emissions using satellite observations of the formaldehyde column, J. Geophys. Res., 111, D12315, doi:10.1029/2005JD006689, 2006. 21477
Paton-Walsh, C., Wilson, S., Jones, N., and Griffith, D.: Measurement of methanol emissions from Australian wildfires by ground-based solar Fourier transform spectroscopy, Geophys. Res. Lett., 35, L08810, doi:10.1029/2006GL027128, 2008. 21479
Paulot, F., Crounse, J. D., Kjaergaard, H. G., Kroll, J. H., Seinfeld, J. H., and Wennberg, P. O.: Isoprene photooxidation: new insights into the production of acids and organic nitrates, Atmos. Chem. Phys., 9, 1479–1501, doi:10.5194/acp-9-1479-2009, 2009. 21481
Perrin, A. and Vander Auwera, J.: An improved database for the 9μm region of the formic acid spectrum, J. Quant. Spectrosc. Rad. Transfer, 108, 363–370, 2007. 21482
Perrin, A., Vander Auwera, J., and Zelinger, Z.: High-resolution Fourier transform study of the ν_3 fundamental band of trans-formic acid, J. Quant. Spectrosc. Rad. Transfer, 110, 743–755, 2009. 21483
Phulpin, T., Blumstein, D., Prel, F., Tournier, B., Prunet, P., and Schlüssel, P.: Applications of IASI on MetOp-A: first results and illustration of potential use for meteorology, climate monitoring and atmospheric chemistry, Proc. SPIE, p. 6684, 2007. 21478
Puxbaum, H., Rosenberg, C., Gregori, M., Lanzerstorfer, C., Ober, E., and Winiwarter, W.: Atmospheric concentrations of formic and acetic acid and related compounds in eastern and northern Austria, Atmos. Environ., 22, 2841–2850, 1988. 21481
Rasmussen, R. and Khalil, M.: Isoprene over the Amazon basin, J. Geophys. Res., 93, 1616, doi:10.1029/JD093iD02p01417, 1988. 21480
Razavi, A., Clerbaux, C., Wespes, C., Clarisse, L., Hurtmans, D., Payan, S., Camy-Peyret, C., and Coheur, P.-F.: Characterization of methane retrievals from the IASI space-borne sounder, Atmos. Chem. Phys., 9, 7889–899, doi:10.5194/acp-9-7889-2009, 2009. 21478
Reiner, T., Möhler, O., and Arnold, F.: Measurements of acetone, acetic acid, and formic acid in the northern midlatitude upper troposphere and lower stratosphere, J. Geophys. Res., 104, 13943, doi:10.1029/1999JD900030, 1999. 21481
Remedios, J., Allen, G., Waterfall, A., Oelhaf, H., Kleinert, A., and Moore, D.: Detection of organic compound signatures in infra-red, limb emission spectra observed by the MIPAS-

ACPD
10, 21475–21519, 2010

B2 balloon instrument, Atmos. Chem. Phys., 7, 1599–1613, doi:10.5194/acp-7-1599-2007, 2007. 21481

Rinsland, C., Mahieu, E., Zander, R., Goldman, A., Wood, S., and Chiou, L.: Free tropospheric measurements of formic acid (HCOOH) from infrared ground-based solar absorption spectra: Retrieval approach, evidence for a seasonal cycle, and comparison with model calculations, J. Geophys. Res., 109, D18308, doi:10.1029/2004JD004917 , 2004. 21477, 21481

Rinsland, C., Dufour, G., Boone, C., Bernath, P., and Chiou, L.: Atmospheric Chemistry Experiment (ACE) measurements of elevated Southern Hemisphere upper tropospheric CO, C_2H_6, HCN, and C_2H_2 mixing ratios from biomass burning emissions and long-range transport, Geophys. Res. Lett., 32, L20803, doi:10.1029/2005GL024214, 2005.

Rinsland, C., Boone, C., Bernath, P., Mahieu, E., Zander, R., Dufour, G., Clerbaux, C., Turquety, S., Chiou, L., Mc-Connell, J., Neary, L., and Kaminski, J. W.: First space-based observations of formic acid (HCOOH): Atmospheric Chemistry Experiment austral spring 2004 and 2005 Southern Hemisphere tropical-mid-latitude upper tropospheric measurements, Geophys. Res. Lett., 33, L23804, doi:10.1029/2006GL027128, 2006. 21477, 21481

Rinsland, C., Dufour, G., Boone, C., Bernath, P., Chiou, L., Coheur, P., Turquety, S., and Clerbaux, C.: Satellite boreal measurements over Alaska and Canada during June-July 2004: Simultaneous measurements of upper tropospheric CO, C_2H_6, HCN, CH_3Cl, CH_4, C_2H_2, CH_3OH, HCOOH, OCS, and SF_6 mixing ratios, Global Biogeochem. Cy., 21, GB3008, doi:10.1029/2006GB002795, 2007. 21477, 21481

Rinsland, C., Mahieu, E., Chiou, L., and Herbin, H.: First ground-based infrared solar absorption measurements of free tropospheric methanol (CH3OH): Multidecade infrared time series from Kitt Peak (31.9° N 111.6° W): Trend, seasonal cycle, and comparison with previous measurements, J. Geophys. Res., 114, D04309, doi:10.1029/2008JD011003, 2009. 21479, 21488

Rodgers, C. D.: Inverse methods for atmospheric sounding: theory and practise, World Sci., River Edge, NJ, USA, 2000, 2000. 21484

Sanhueza, E. and Andreae, M.: Emission of formic and acetic acids from tropical savanna soils, Geophys. Res. Lett., 18, 1707–1710, 1991. 21480

Sanhueza, E., Figueroa, L., and Santana, M.: Atmospheric formic and acetic acids in Venezuela, Atmos. Environ., 30, 1861–1873, 1996. 21480

Schade, G. and Goldstein, A.: Seasonal measurements of acetone and methanol: Abundances and implications for atmospheric budgets, Global Biogeochem. Cy., 20, GB1011,

ACPD

10, 21475–21519, 2010

doi:10.1029/2005GB002566, 2006. 21479, 21488
Shim, C., Wang, Y., Choi, Y., Palmer, P., Abbot, D., and Chance, K.: Constraining global isoprene emissions with Global Ozone Monitoring Experiment (GOME) formaldehyde column measurements, J. Geophys. Res., 110, D24301, doi:10.1029/2004JD005629, 2005. 21477
Singh, H., Chen, Y., Tabazadeh, A., Fukui, Y., Bey, I., Yantosca, R., Jacob, D., Arnold, F., Wohlfrom, K., Atlas, E., et al.: Distribution and fate of selected oxygenated organic species in the troposphere and lower stratosphere over the Atlantic, J. Geophys. Res., 105, 3795–3805, 2000. 21479, 21481
Singh, H., Salas, L., Chatfield, R., Czech, E., Fried, A., Walega, J., Evans, M., Field, B., Jacob, D., Blake, D., Heikes, B., Talbot, R., Sachse, G., Crawford, J., Avery, M., Sandholm, S., and Fuelberg, H.: Analysis of the atmospheric distribution, sources, and sinks of oxygenated volatile organic chemicals based on measurements over the Pacific during TRACE-P, J. Geophys. Res., 109, D15S07, doi:10.1029/2003JD003883, 2004. 21479
Souza, S., Vasconcellos, P., and Carvalho, L.: Low molecular weight carboxylic acids in an urban atmosphere: Winter measurements in Sao Paulo City, Brazil, Atmos. Environ., 33, 2563–2574, 1999. 21481
Stavrakou, T., Müller, J.-F., De Smedt, I., Van Roozendael, M., van der Werf, G. R., Giglio, L., and Guenther, A.: Global emissions of non-methane hydrocarbons deduced from SCIAMACHY formaldehyde columns through 2003-2006, Atmos. Chem. Phys., 9, 3663–3679, doi:10.5194/acp-7-1599-2007, 2009. 21477, 21485
Talbot, R., Beecher, K., and Harriss, R.: Atmospheric geochemistry of formic and acetic acids at a mid-latitude temperate site, J. Geophys. Res., 93, 1638–1652, 1988. 21481
Talbot, R., Andreae, M., Berresheim, H., Jacob, D., and Beecher, K.: Sources and sinks of formic, acetic, and pyruvic acids over central Amazonia 2. Wet season, J. Geophys. Res., 95, 799–816, 1990. 21481
Tie, X., Guenther, A., and Holland, E.: Biogenic methanol and its impacts on tropospheric oxidants, Geophys. Res. Lett, 30(17), p. 1881, doi:10.1029/2003GL017167, 2003. 21478, 21479
Tsigaridis, K. and Kanakidou, M.: Secondary organic aerosol importance in the future atmosphere, Atmos. Environ., 41, 4682–4692, 2007. 21477
Turquety, S., Hurtmans, D., Hadji-Lazaro, J., Coheur, P.-F., Clerbaux, C., Josset, D., and Tsamalis, C.: Tracking the emission and transport of pollution from wildfires using the IASI CO retrievals: analysis of of the summer 2007 Greek fires, Atmos. Chem. Phys., 9, 4897–

ACPD
10, 21475–21519, 2010

4913, doi:10.5194/acp-9-4897-2009, 2009. 21478
Vander Auwera, J., Didriche, K., Perrin, A., and Keller, F.: Absolute line intensities for formic acid and dissociation constant of the dimer, The J. Chem. Phys., 126, 124311, doi:10.1063/1.2712439, 2007. 21482, 21492
Vrekoussis, M., Wittrock, F., Richter, A., and Burrows, J. P.: Temporal and spatial variability of glyoxal as observed from space, Atmos. Chem. Phys., 9, 4485–4504, doi:10.5194/acp-9-4485-2009, 2009. 21478
Warneke, C., Karl, T., Judmaier, H., Hansel, A., Jordan, A., Lindinger, W., and Crutzen, P.: Acetone, methanol, and other partially oxidized volatile organic emissions from dead plant matter by abiological processes: Significance for atmospheric HO_x chemistry, Global Biogeochem. Cy., 13, 9–17, 1999. 21479
Wespes, C., Hurtmans, D., Clerbaux, C., Santee, M. L., Martin, R. V., and Coheur, P.-F.: Global distributions of nitric acid from IASI/MetOP measurements, Atmos. Chem. Phys., 9, 7949–7962, doi:10.5194/acp-9-7949-2009, 2009. 21478
Wilber, A., Kratz, D., and Gupta, S.: Surface emissivity maps for use in satellite retrievals of longwave radiation, NASA Tech. Publ., 209362, 35, 1999. 21488
Wittrock, F., Richter, A., Oetjen, H., Burrows, J., Kanakidou, M., Myriokefalitakis, S., Volkamer, R., Beirle, S., Platt, U., and Wagner, T.: Simultaneous global observations of glyoxal and formaldehyde from space, Geophys. Res. Lett., 33, L16804, doi:10.1029/2006GL026310, 2006. 21478
Worden, H., Beer, R., and Rinsland, C.: Airborne infrared spectroscopy of 1994 western wildfires, J. Geophys. Res., 102, 1287–1300, 1997. 21480, 21481, 21492
Yokelson, R., Susott, R., Ward, D., Reardon, J., and Griffith, D.: Emissions from smoldering combustion of biomass measured by open-path Fourier transform infrared spectroscopy, J. Geophys. Res., 102(18), 18865–18877, doi:10.1029/97JD00852, 1997. 21480
Yokelson, R., Goode, J., Ward, D., Susott, R., Babbitt, R., Wade, D., Bertschi, I., Griffith, D., and Hao, W.: Emissions of formaldehyde, acetic acid, methanol, and other trace gases from biomass fires in North Carolina measured by airborne Fourier transform infrared spectroscopy, J. Geophys. Res., 104, 30109, doi:10.1029/1999JD900817, 1999. 21479, 21481, 21494
Yokelson, R., Bertschi, I., Christian, T., Hobbs, P., Ward, D., and Hao, W.: Trace gas measurements in nascent, aged, and cloud-processed smoke from African savanna fires by airborne Fourier transform infrared spectroscopy (AFTIR), J. Geophys. Res., 108, 8478,

ACPD
10, 21475–21519, 2010

doi:10.1029/2002JD002322, 2003. 21479
Zander, R., Duchatelet, P., Mahieu, E., Demoulin, P., Roland, G., Servais, C., Vander Auwera, J., Perrin, A., Rinsland, C., and Crutzen, P.: Formic acid above the Jungfraujoch during 1985–2007: observed variability, seasonality, but no long-term background evolution, Atmos. Chem. Phys. Discuss., 10, 14771–14814, doi:10.5194/acpd-10-14771-2010, 2010. 21481

ACPD
10, 21475–21519, 2010

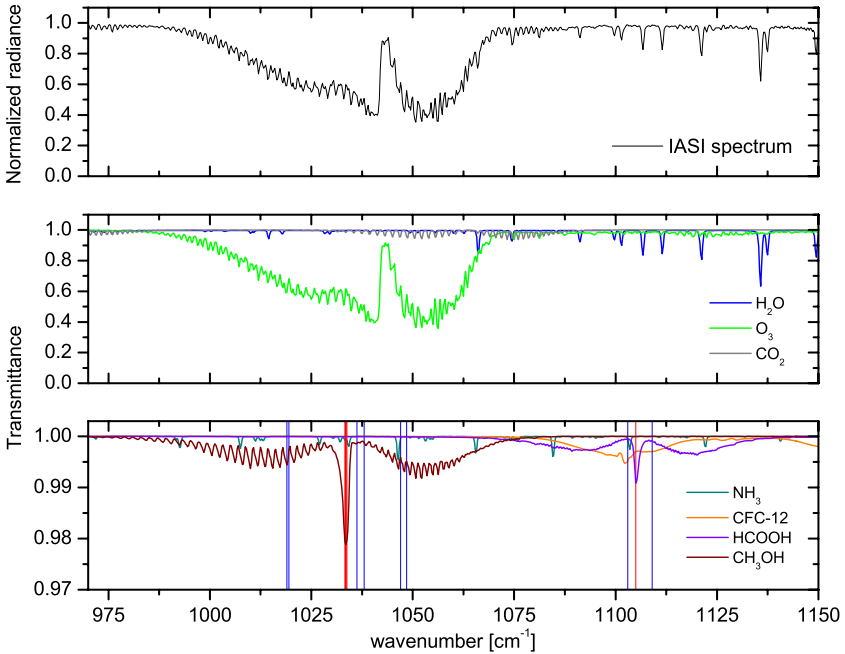

Fig. 1. *Top panel* IASI normalized radiance spectrum in the spectral region between 950 and 1200 cm^{-1} containing methanol and formic acid absorption bands. *Bottom panels* Contribution to the IASI spectrum of different atmospheric species plotted in transmittance. The vertical lines indicate the target channels (in red) and the baseline channels (in blue) which are used for the ΔT_b determination (nine channels are used for CH_3OH, and three for HCOOH). See Sect. 2.2 for details.

ACPD
10, 21475–21519, 2010

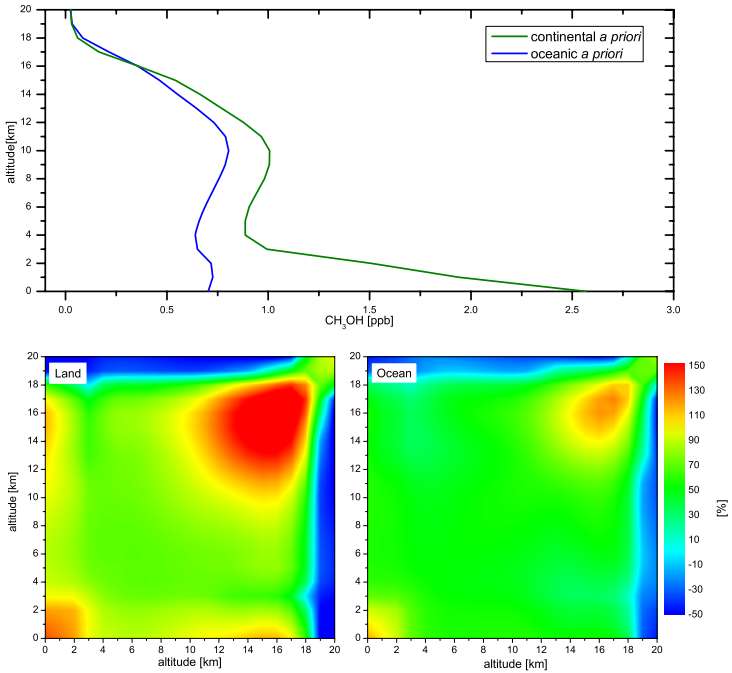

Fig. 2. *Top panel* Illustration of the two CH_3OH a priori profiles (continental and oceanic) derived from the IMAGESv2 CTM model for the year 2007. *Bottom panel* Plot (expressed in %) of the associated covariance matrices (left: land, right: ocean) that illustrates the variability through the diagonal elements and the correlation between the different levels with off-diagonal values.

ACPD
10, 21475–21519, 2010

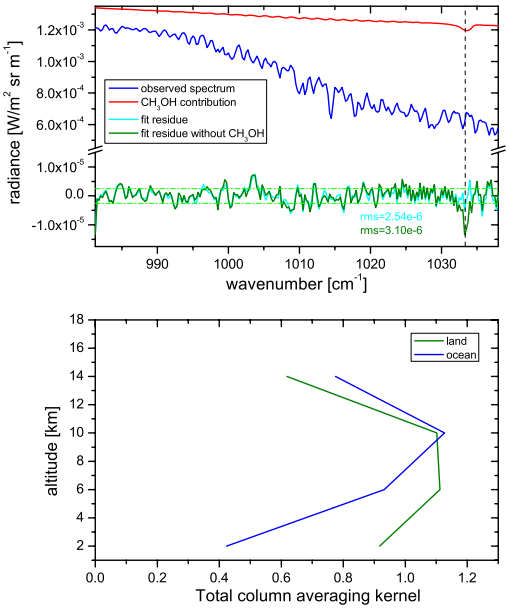

Fig. 3. *Top panel* Example of a methanol retrieval from an IASI spectrum recorded over Namibia (20.16° S–21.50° E) on October 20, 2008. The observed (blue curve) spectrum is shown together with the fit residue (in cyan). The dark green curve is the fit residue when CH_3OH is not taken into account in the retrieval, the red curve represents the calculated CH_3OH contribution to the spectrum and the dashed vertical line indicates the detectable CH_3OH absorption band. *Bottom panel* Mean total column averaging kernels presented for retrievals performed over land (green curve) and over ocean (blue curve).

ACPD
10, 21475–21519, 2010

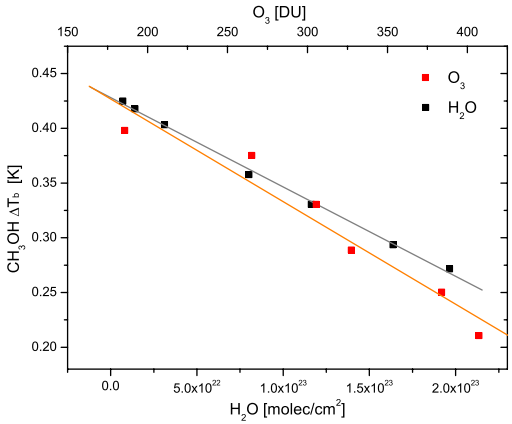

Fig. 4. Illustration of the influence of water vapor and ozone concentrations on the methanol ΔT_b. Simulations were performed for the midlatitude summer model with varying concentrations of H_2O (black squares) and O_3 (red squares) while the CH_3OH amount was fixed. In both cases, a linear dependence is found.

ACPD
10, 21475–21519, 2010

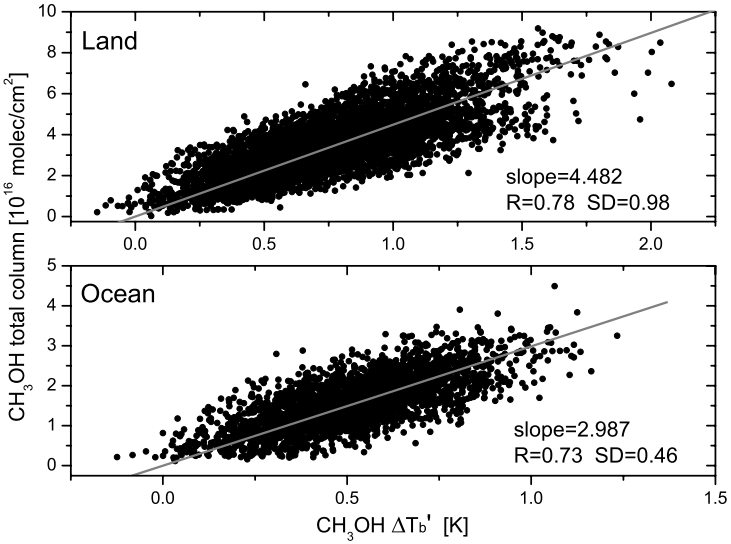

Fig. 5. Correlation between the retrieved total columns of methanol and the corresponding ΔT_b for various regions (corrected for O_3 and H_2O dependency, see text for details). The conversion factors are given by the slopes of the linear fit (gray curve) separated for retrievals above land (*Top panel*) and above ocean (*Bottom panel*).

ACPD
10, 21475–21519, 2010

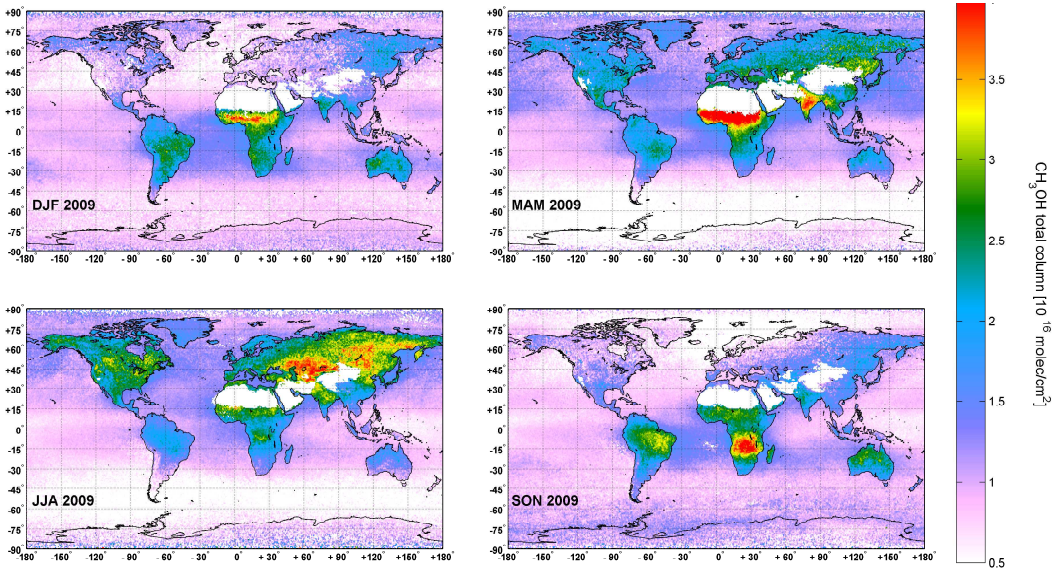

Fig. 6. Seasonal distributions of methanol total columns for the year 2009. The white areas correspond to a filter for sandy scenes where emissivity is uncertain.

ACPD
10, 21475–21519, 2010

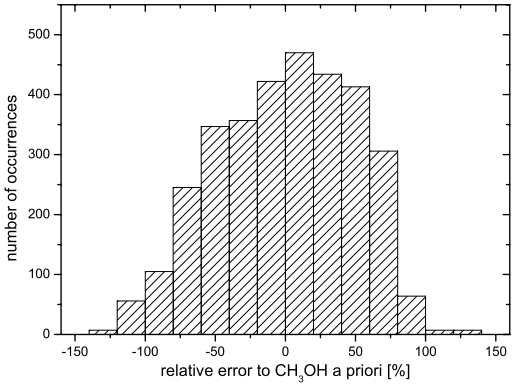

Fig. 7. Histogram of the relative errors between the simulated CH_3OH total columns and the total columns derived from the ΔT_b calculation.

ACPD
10, 21475–21519, 2010

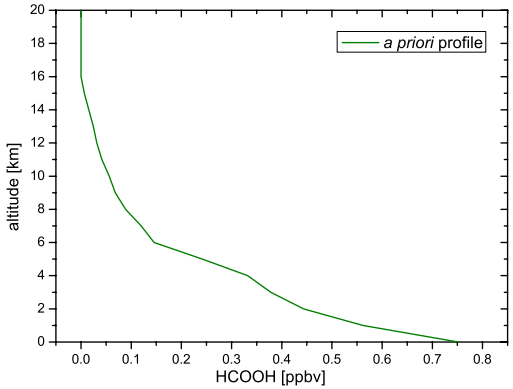

Fig. 8. HCOOH a priori profile derived from the combined aircraft and ACE measurements. See text for details.

ACPD
10, 21475–21519, 2010

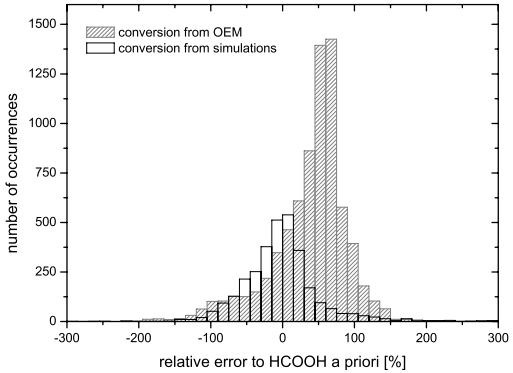

Fig. 9. Histograms of the relative error between the simulated total columns of HCOOH and the HCOOH total columns obtained from brightness temperature differences. The gray histogram is derived from the conversion which uses OEM retrievals and the black one corresponds to the conversion obtained with simulated data. The latter, which is much less biased is used to obtain the global distributions (see Sect. 4.2).

ACPD
10, 21475–21519, 2010

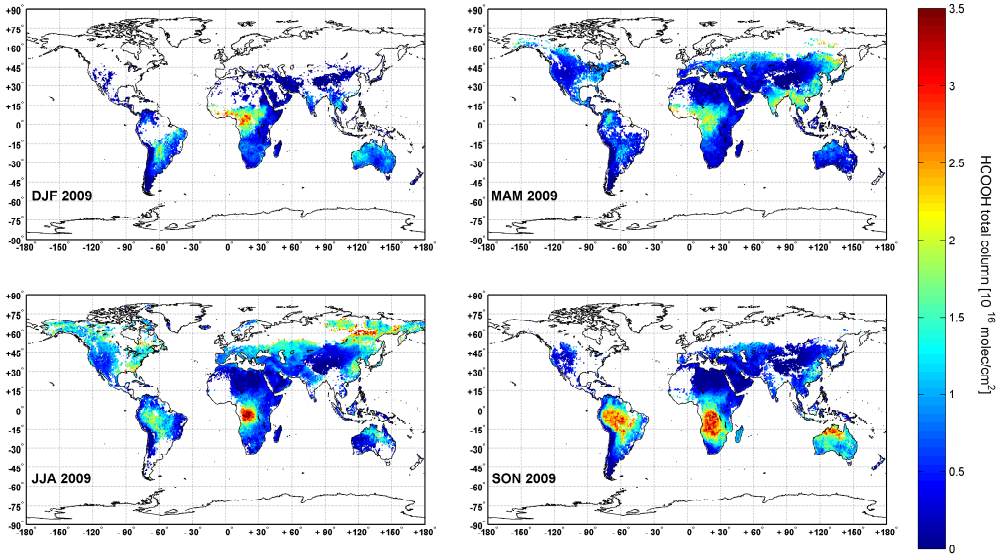

Fig. 10. Seasonal distributions of formic acid total columns for the year 2009. Only cloud free observations recorded during daytime above continents along with a thermal contrast higher than 5 K were considered.

ACPD
10, 21475–21519, 2010

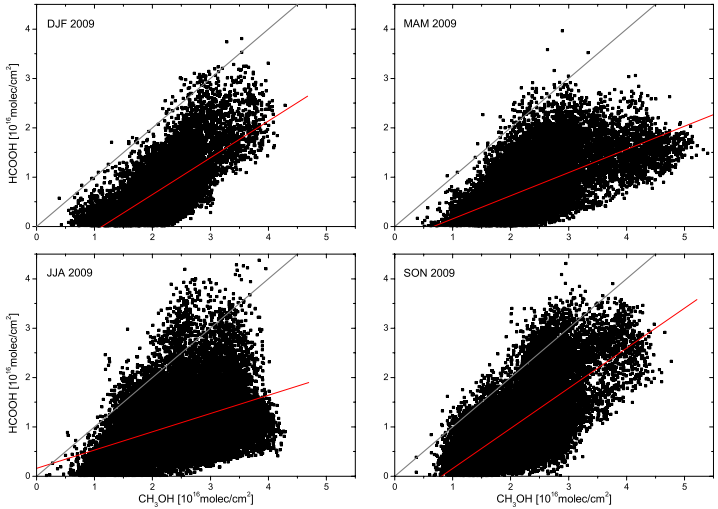

Fig. 11. Global correlations between methanol and formic acid total columns differentiated for each season of the year 2009. The resulting linear fit is represented in red. The one to one line is shown in gray.

ACPD
10, 21475–21519, 2010

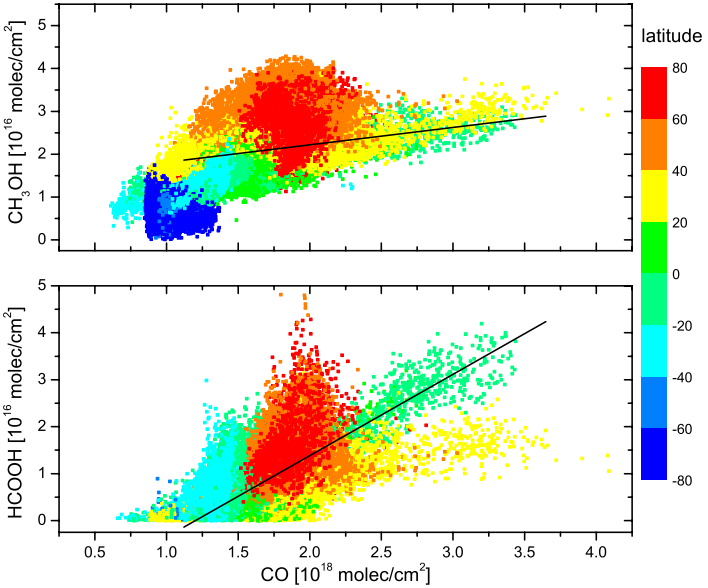

Fig. 12. Continental correlations of CO with CH_3OH (*Top panel*) and with HCOOH (*Bottom panel*) presented for the 3 month period of summer 2009. The colors represent different latitudinal bands of 20° width and the black lines correspond to a correlation between the two species in regions where the biomass burning source is dominant (see text for more details).

ACPD
10, 21475–21519, 2010